

Search for $B^0 \rightarrow \rho^0 \rho^0$ and Non-Resonant $B^0 \rightarrow 4\pi$ Decays

K. Abe,¹⁰ I. Adachi,¹⁰ H. Aihara,⁵² K. Arinstein,¹ T. Aso,⁵⁶ V. Aulchenko,¹
T. Aushev,^{22,16} T. Aziz,⁴⁸ S. Bahinipati,³ A. M. Bakich,⁴⁷ V. Balagura,¹⁶ Y. Ban,³⁸
S. Banerjee,⁴⁸ E. Barberio,²⁵ A. Bay,²² I. Bedny,¹ K. Belous,¹⁵ V. Bhardwaj,³⁷
U. Bitenc,¹⁷ S. Blyth,²⁹ A. Bondar,¹ A. Bozek,³¹ M. Bračko,^{24,17} J. Brodzicka,¹⁰
T. E. Browder,⁹ M.-C. Chang,⁴ P. Chang,³⁰ Y. Chao,³⁰ A. Chen,²⁸ K.-F. Chen,³⁰
W. T. Chen,²⁸ B. G. Cheon,⁸ C.-C. Chiang,³⁰ R. Chistov,¹⁶ I.-S. Cho,⁵⁸ S.-K. Choi,⁷
Y. Choi,⁴⁶ Y. K. Choi,⁴⁶ S. Cole,⁴⁷ J. Dalseno,²⁵ M. Danilov,¹⁶ A. Das,⁴⁸ M. Dash,⁵⁷
J. Dragic,¹⁰ A. Drutskoy,³ S. Eidelman,¹ D. Epifanov,¹ S. Fratina,¹⁷ H. Fujii,¹⁰
M. Fujikawa,²⁷ N. Gabyshev,¹ A. Garmash,⁴⁰ A. Go,²⁸ G. Gokhroo,⁴⁸ P. Goldenzweig,³
B. Golob,^{23,17} M. Grosse Perdekamp,^{12,41} H. Guler,⁹ H. Ha,¹⁹ J. Haba,¹⁰ K. Hara,²⁶
T. Hara,³⁶ Y. Hasegawa,⁴⁵ N. C. Hastings,⁵² K. Hayasaka,²⁶ H. Hayashii,²⁷ M. Hazumi,¹⁰
D. Heffernan,³⁶ T. Higuchi,¹⁰ L. Hinz,²² H. Hoedlmoser,⁹ T. Hokuue,²⁶ Y. Horii,⁵¹
Y. Hoshi,⁵⁰ K. Hoshina,⁵⁵ S. Hou,²⁸ W.-S. Hou,³⁰ Y. B. Hsiung,³⁰ H. J. Hyun,²¹
Y. Igarashi,¹⁰ T. Iijima,²⁶ K. Ikado,²⁶ K. Inami,²⁶ A. Ishikawa,⁴² H. Ishino,⁵³ R. Itoh,¹⁰
M. Iwabuchi,⁶ M. Iwasaki,⁵² Y. Iwasaki,¹⁰ C. Jacoby,²² N. J. Joshi,⁴⁸ M. Kaga,²⁶
D. H. Kah,²¹ H. Kaji,²⁶ S. Kajiwara,³⁶ H. Kakuno,⁵² J. H. Kang,⁵⁸ P. Kapusta,³¹
S. U. Kataoka,²⁷ N. Katayama,¹⁰ H. Kawai,² T. Kawasaki,³³ A. Kibayashi,¹⁰
H. Kichimi,¹⁰ H. J. Kim,²¹ H. O. Kim,⁴⁶ J. H. Kim,⁴⁶ S. K. Kim,⁴⁴ Y. J. Kim,⁶
K. Kinoshita,³ S. Korpar,^{24,17} Y. Kozakai,²⁶ P. Križan,^{23,17} P. Krokovny,¹⁰ R. Kumar,³⁷
E. Kurihara,² A. Kusaka,⁵² A. Kuzmin,¹ Y.-J. Kwon,⁵⁸ J. S. Lange,⁵ G. Leder,¹⁴
J. Lee,⁴⁴ J. S. Lee,⁴⁶ M. J. Lee,⁴⁴ S. E. Lee,⁴⁴ T. Lesiak,³¹ J. Li,⁹ A. Limosani,²⁵
S.-W. Lin,³⁰ Y. Liu,⁶ D. Liventsev,¹⁶ J. MacNaughton,¹⁰ G. Majumder,⁴⁸ F. Mandl,¹⁴
D. Marlow,⁴⁰ T. Matsumura,²⁶ A. Matyja,³¹ S. McOnie,⁴⁷ T. Medvedeva,¹⁶ Y. Mikami,⁵¹
W. Mitaroff,¹⁴ K. Miyabayashi,²⁷ H. Miyake,³⁶ H. Miyata,³³ Y. Miyazaki,²⁶ R. Mizuk,¹⁶
G. R. Moloney,²⁵ T. Mori,²⁶ J. Mueller,³⁹ A. Murakami,⁴² T. Nagamine,⁵¹ Y. Nagasaka,¹¹
Y. Nakahama,⁵² I. Nakamura,¹⁰ E. Nakano,³⁵ M. Nakao,¹⁰ H. Nakayama,⁵²
H. Nakazawa,²⁸ Z. Natkaniec,³¹ K. Neichi,⁵⁰ S. Nishida,¹⁰ K. Nishimura,⁹ Y. Nishio,²⁶
I. Nishizawa,⁵⁴ O. Nitoh,⁵⁵ S. Noguchi,²⁷ T. Nozaki,¹⁰ A. Ogawa,⁴¹ S. Ogawa,⁴⁹
T. Ohshima,²⁶ S. Okuno,¹⁸ S. L. Olsen,⁹ S. Ono,⁵³ W. Ostrowicz,³¹ H. Ozaki,¹⁰
P. Pakhlov,¹⁶ G. Pakhlova,¹⁶ H. Palka,³¹ C. W. Park,⁴⁶ H. Park,²¹ K. S. Park,⁴⁶
N. Parslow,⁴⁷ L. S. Peak,⁴⁷ M. Pernicka,¹⁴ R. Pestotnik,¹⁷ M. Peters,⁹ L. E. Piilonen,⁵⁷
A. Poluektov,¹ J. Rorie,⁹ M. Rozanska,³¹ H. Sahoo,⁹ Y. Sakai,¹⁰ H. Sakamoto,²⁰
H. Sakaue,³⁵ T. R. Sarangi,⁶ N. Satoyama,⁴⁵ K. Sayeed,³ T. Schietinger,²²
O. Schneider,²² P. Schönmeier,⁵¹ J. Schümann,¹⁰ C. Schwanda,¹⁴ A. J. Schwartz,³
R. Seidl,^{12,41} A. Sekiya,²⁷ K. Senyo,²⁶ M. E. Sevier,²⁵ L. Shang,¹³ M. Shapkin,¹⁵
C. P. Shen,¹³ H. Shibuya,⁴⁹ S. Shinomiya,³⁶ J.-G. Shiu,³⁰ B. Shwartz,¹ J. B. Singh,³⁷

A. Sokolov,¹⁵ E. Solovieva,¹⁶ A. Somov,³ S. Stanič,³⁴ M. Starič,¹⁷ J. Stypula,³¹
A. Sugiyama,⁴² K. Sumisawa,¹⁰ T. Sumiyoshi,⁵⁴ S. Suzuki,⁴² S. Y. Suzuki,¹⁰ O. Tajima,¹⁰
F. Takasaki,¹⁰ K. Tamai,¹⁰ N. Tamura,³³ M. Tanaka,¹⁰ N. Taniguchi,²⁰ G. N. Taylor,²⁵
Y. Teramoto,³⁵ I. Tikhomirov,¹⁶ K. Trabelsi,¹⁰ Y. F. Tse,²⁵ T. Tsuboyama,¹⁰ K. Uchida,⁹
Y. Uchida,⁶ S. Uehara,¹⁰ K. Ueno,³⁰ T. Uglov,¹⁶ Y. Unno,⁸ S. Uno,¹⁰ P. Urquijo,²⁵
Y. Ushiroda,¹⁰ Y. Usov,¹ G. Varner,⁹ K. E. Varvell,⁴⁷ K. Vervink,²² S. Villa,²²
A. Vinokurova,¹ C. C. Wang,³⁰ C. H. Wang,²⁹ J. Wang,³⁸ M.-Z. Wang,³⁰ P. Wang,¹³
X. L. Wang,¹³ M. Watanabe,³³ Y. Watanabe,¹⁸ R. Wedd,²⁵ J. Wicht,²² L. Widhalm,¹⁴
J. Wiechczynski,³¹ E. Won,¹⁹ B. D. Yabsley,⁴⁷ A. Yamaguchi,⁵¹ H. Yamamoto,⁵¹
M. Yamaoka,²⁶ Y. Yamashita,³² M. Yamauchi,¹⁰ C. Z. Yuan,¹³ Y. Yusa,⁵⁷ C. C. Zhang,¹³
L. M. Zhang,⁴³ Z. P. Zhang,⁴³ V. Zhilich,¹ V. Zhulanov,¹ A. Zupanc,¹⁷ and N. Zwahlen²²

(The Belle Collaboration)

¹*Budker Institute of Nuclear Physics, Novosibirsk*

²*Chiba University, Chiba*

³*University of Cincinnati, Cincinnati, Ohio 45221*

⁴*Department of Physics, Fu Jen Catholic University, Taipei*

⁵*Justus-Liebig-Universität Gießen, Gießen*

⁶*The Graduate University for Advanced Studies, Hayama*

⁷*Gyeongsang National University, Chinju*

⁸*Hanyang University, Seoul*

⁹*University of Hawaii, Honolulu, Hawaii 96822*

¹⁰*High Energy Accelerator Research Organization (KEK), Tsukuba*

¹¹*Hiroshima Institute of Technology, Hiroshima*

¹²*University of Illinois at Urbana-Champaign, Urbana, Illinois 61801*

¹³*Institute of High Energy Physics,*

Chinese Academy of Sciences, Beijing

¹⁴*Institute of High Energy Physics, Vienna*

¹⁵*Institute of High Energy Physics, Protvino*

¹⁶*Institute for Theoretical and Experimental Physics, Moscow*

¹⁷*J. Stefan Institute, Ljubljana*

¹⁸*Kanagawa University, Yokohama*

¹⁹*Korea University, Seoul*

²⁰*Kyoto University, Kyoto*

²¹*Kyungpook National University, Taegu*

²²*Ecole Polytechnique Fédérale Lausanne, EPFL, Lausanne*

²³*University of Ljubljana, Ljubljana*

²⁴*University of Maribor, Maribor*

²⁵*University of Melbourne, School of Physics, Victoria 3010*

²⁶*Nagoya University, Nagoya*

²⁷*Nara Women's University, Nara*

²⁸*National Central University, Chung-li*

²⁹*National United University, Miao Li*

³⁰*Department of Physics, National Taiwan University, Taipei*

³¹*H. Niewodniczanski Institute of Nuclear Physics, Krakow*

³²*Nippon Dental University, Niigata*

- ³³*Niigata University, Niigata*
³⁴*University of Nova Gorica, Nova Gorica*
³⁵*Osaka City University, Osaka*
³⁶*Osaka University, Osaka*
³⁷*Panjab University, Chandigarh*
³⁸*Peking University, Beijing*
³⁹*University of Pittsburgh, Pittsburgh, Pennsylvania 15260*
⁴⁰*Princeton University, Princeton, New Jersey 08544*
⁴¹*RIKEN BNL Research Center, Upton, New York 11973*
⁴²*Saga University, Saga*
⁴³*University of Science and Technology of China, Hefei*
⁴⁴*Seoul National University, Seoul*
⁴⁵*Shinshu University, Nagano*
⁴⁶*Sungkyunkwan University, Suwon*
⁴⁷*University of Sydney, Sydney, New South Wales*
⁴⁸*Tata Institute of Fundamental Research, Mumbai*
⁴⁹*Toho University, Funabashi*
⁵⁰*Tohoku Gakuin University, Tagajo*
⁵¹*Tohoku University, Sendai*
⁵²*Department of Physics, University of Tokyo, Tokyo*
⁵³*Tokyo Institute of Technology, Tokyo*
⁵⁴*Tokyo Metropolitan University, Tokyo*
⁵⁵*Tokyo University of Agriculture and Technology, Tokyo*
⁵⁶*Toyama National College of Maritime Technology, Toyama*
⁵⁷*Virginia Polytechnic Institute and State University, Blacksburg, Virginia 24061*
⁵⁸*Yonsei University, Seoul*

Abstract

We search for the decay $B^0 \rightarrow \rho^0 \rho^0$ and other possible charmless modes with a $\pi^+ \pi^- \pi^+ \pi^-$ final state, including $B^0 \rightarrow \rho^0 f_0(980)$, $B^0 \rightarrow f_0(980) f_0(980)$, $B^0 \rightarrow f_0(980) \pi \pi$, $B^0 \rightarrow \rho^0 \pi \pi$ and non-resonant $B^0 \rightarrow 4\pi$. These results are obtained from a data sample containing 520×10^6 $B\bar{B}$ pairs collected by the Belle detector at the KEKB asymmetric-energy e^+e^- collider. We measure a branching fraction of $(0.9 \pm 0.4^{+0.3}_{-0.4}) \times 10^{-6}$, or $\mathcal{B}(B^0 \rightarrow \rho^0 \rho^0) < 1.6 \times 10^{-6}$ at the 90% confidence level. The significance including systematic uncertainties is 1.8σ . These values correspond to the final state being longitudinally polarized. We also measure the branching fraction of non-resonant $B^0 \rightarrow 4\pi$ decay to be $(10.2 \pm 4.7^{+2.3}_{-1.5}) \times 10^{-6}$ with 2.1σ significance, and set the 90% confidence level upper limit $\mathcal{B}(B^0 \rightarrow 4\pi) < 17.3 \times 10^{-6}$. For the other related decays, $B^0 \rightarrow \rho^0 f_0(980)$, $B^0 \rightarrow f_0(980) f_0(980)$, $B^0 \rightarrow f_0(980) \pi \pi$ and $B^0 \rightarrow \rho^0 \pi \pi$, no significant signals are observed and upper limits on the branching fractions are set.

PACS numbers: 11.30.Er, 12.15.Hh, 13.25.Hw, 14.40.Nd

INTRODUCTION

In the Standard Model (SM), CP violation in the weak interaction can be measured through the differences between B and \bar{B} mesons decays. Measurements of CP violation help determine (or constrain) the elements of the Cabibbo-Kobayashi-Maskawa (CKM) quark-mixing matrix [1] and thus test the Standard Model. The time-dependent CP asymmetry for the decay of a neutral B meson via a $b \rightarrow u$ process into a CP eigenstate can determine the CKM phase angle $\phi_2 \equiv -\frac{V_{td}V_{tb}^*}{V_{ud}V_{ub}^*}$. However, in addition to the $b \rightarrow u$ tree amplitude, a $b \rightarrow d$ penguin amplitude contributions, and thus an isospin analysis [2] is needed to determine ϕ_2 .

At present, the ϕ_2 constraints on $B \rightarrow \pi\pi$ [3], $B \rightarrow \rho\pi$ [4] and $B \rightarrow \rho\rho$ [5] are well studied. However, it is necessary to measure the branching fraction and polarization of $B^0 \rightarrow \rho^0\rho^0$ for improved ϕ_2 constraints. Angular analysis can provide additional information on VV decays such as $B \rightarrow \rho\rho$. Polarization measurements in the $B^0 \rightarrow \rho^+\rho^-$ and $B^+ \rightarrow \rho^+\rho^0$ modes [5] show the dominance of longitudinal polarization, thus $B^0 \rightarrow \rho^+\rho^-$ is a CP eigenstate; measurements of the branching fraction and polarization of CP -violating asymmetry in $B^0 \rightarrow \rho^0\rho^0$ decays would complete the isospin triangle and improve the constraints on ϕ_2 .

Theoretically, the tree contribution to $B^0 \rightarrow \rho^0\rho^0$ is color-suppressed and thus its branching fraction is much smaller than that of $B^0 \rightarrow \rho^+\rho^-$ or $B^+ \rightarrow \rho^+\rho^0$. The decay rate for $\rho^0\rho^0$ is sensitive to the penguin amplitude. Predictions for $B^0 \rightarrow \rho^0\rho^0$ using perturbative QCD (pQCD) [6] or QCD factorization [7, 8] approaches suggest that the branching fraction $\mathcal{B}(B^0 \rightarrow \rho^0\rho^0)$ is at or below 1×10^{-6} and that the longitudinal polarization fraction, f_L , is around 0.85. A non-zero branching fraction for $B^0 \rightarrow \rho^0\rho^0$ was first reported by the BaBar collaboration [9]; they measured a branching fraction of $\mathcal{B}(B^0 \rightarrow \rho^0\rho^0) = (1.07 \pm 0.33 \pm 0.19) \times 10^{-6}$ with a significance of 3.5 standard deviations (σ), and a longitudinal polarization fraction, $f_L = 0.87 \pm 0.13 \pm 0.04$.

A theoretical prediction for the non-resonant $B^0 \rightarrow 4\pi$ branching fraction is around 1×10^{-4} [10]. The most recent measurement of this decay was made by the DELPHI collaboration [11], who set a 90% confidence level upper limit on the branching fraction of 2.3×10^{-4} .

In this paper, we report the results of a search for $B^0 \rightarrow \rho^0\rho^0$ along with other modes, including $B^0 \rightarrow \rho^0 f_0$, $B^0 \rightarrow f_0 f_0$, $B^0 \rightarrow f_0 \pi\pi$, $B^0 \rightarrow \rho^0 \pi\pi$ and non-resonant $B^0 \rightarrow 4\pi$.

DATA SET AND APPARATUS

The data sample used contains 520×10^6 $B\bar{B}$ pairs collected with the Belle detector at the KEKB asymmetric-energy e^+e^- (3.5 and 8 GeV) collider [12], operating at the $\Upsilon(4S)$ resonance. The Belle detector [13, 14] is a large-solid-angle magnetic spectrometer that consists of a silicon vertex detector, a 50-layer central drift chamber (CDC), an array of aerogel threshold Cherenkov counters (ACC), a barrel-like arrangement of time-of-flight scintillation counters (TOF), and an electromagnetic calorimeter comprised of CsI(Tl) crystals (ECL) located inside a superconducting solenoid coil that provides a 1.5 T magnetic field. An iron flux-return located outside of the coil is instrumented to detect K_L^0 mesons and to identify muons.

We study signal and backgrounds using Monte Carlo (MC) simulation. For these simulations, signal decays, generic $b \rightarrow c$ decays and charmless rare B decays are generated

with the EVTGEN [15] event generator. Signal MC event generation utilizes the PHOTOS simulation package to take account of final-state radiation [16]. The continuum MC events are generated through $e^+e^- \rightarrow \gamma^* \rightarrow q\bar{q}$ ($q = u, d, s, c$) decays in JETSET [17]. The GEANT3 [18] package is used for detector simulation.

EVENT SELECTION AND RECONSTRUCTION

B^0 meson candidates are reconstructed from neutral combinations of four charged pions. Charged track candidates are required to have a distance-of-closest-approach to the interaction point (IP) of less than 2 cm in the beam direction (z -axis) and less than 0.1 cm in the transverse plane; they are also required to have a transverse momentum $p_T > 0.1$ GeV/ c in the laboratory frame. Charged pions are identified using particle identification (PID) information obtained from the the CDC (dE/dx), the ACC and the TOF. We distinguish charged kaons and pions using a likelihood ratio $\mathcal{R}_{\text{PID}} = \mathcal{L}_K/(\mathcal{L}_K + \mathcal{L}_\pi)$, where \mathcal{L}_π (\mathcal{L}_K) is a likelihood value for the pion (kaon) hypothesis. We require $\mathcal{R}_{\text{PID}} < 0.4$ for the four charged pions. The pion identification efficiency is 90%, and 12% of kaons are misidentified as pions. Charged particles positively identified as an electron or a muon are removed.

To veto $B \rightarrow D^{(*)}\pi$ backgrounds, we remove candidates that satisfy any one of the following conditions: $|M(h^\pm\pi^\mp\pi^\mp) - M_{D_{(s)}}| < 13$ MeV/ c^2 or $|M(h^\pm\pi^\mp) - M_{D^0}| < 13$ MeV/ c^2 , where h^\pm is either a pion or a kaon, and $M_{D_{(s)}}$ and M_{D^0} are the nominal masses of $D_{(s)}$ and D^0 , respectively. Furthermore, to reduce the $B^0 \rightarrow a_1^\pm\pi^\mp$ feeddown in the signal region (0.55 GeV/ $c^2 < M_{1,2}(\pi\pi) < 1.35$ GeV/ c^2), we require that the highest momentum pion have a momentum in the $\Upsilon(4S)$ center-of-mass (CM) frame within the range 1.30-2.65 GeV/ c .

The signal event candidates are characterized by two kinematic variables: beam-energy constrained mass, $M_{\text{bc}} = \sqrt{E_{\text{beam}}^2 - P_B^2}$, and energy difference, $\Delta E = E_B - E_{\text{beam}}$, where E_{beam} is the run-dependent beam energy, P_B and E_B are the momentum and energy of the B candidate in the $\Upsilon(4S)$ CM frame. We select candidate events in the region 5.24 GeV/ $c^2 < M_{\text{bc}} < 5.30$ GeV/ c^2 and $|\Delta E| < 0.01$ GeV.

The invariant masses $M_1(\pi^+\pi^-)$ and $M_2(\pi^+\pi^-)$, are used to distinguish different modes from signal. In $B^0 \rightarrow \rho^0\rho^0 \rightarrow (\pi^+\pi^-)(\pi^+\pi^-)$ decays, there are two possible combinations: $(\pi_1^+\pi_1^-)(\pi_2^+\pi_2^-)$ and $(\pi_1^+\pi_2^-)(\pi_2^+\pi_1^-)$, where the subscripts label the momentum ordering (e.g., π_1^+ has higher momentum than π_2^+). According to a MC study, assuming $B^0 \rightarrow \rho^0\rho^0$ decays are longitudinally polarized, the reconstructed $\pi^+\pi^-$ pair containing a high momentum $\pi^+(\pi^-)$ and a low momentum $\pi^-(\pi^+)$ will corresponds to the correct combination 84.8% of the time. Here we consider both possible $\pi^+\pi^-$ combinations and select candidate events if either one of the combinations lies in the $\rho^0\rho^0$ signal mass window, which is 0.55 GeV/ $c^2 < M(\pi_1^+\pi_1^-) \cap M(\pi_2^+\pi_2^-) < 1.35$ GeV/ c^2 or 0.55 GeV/ $c^2 < M(\pi_1^+\pi_2^-) \cap M(\pi_2^+\pi_1^-) < 1.35$ GeV/ c^2 . If a candidate event has two $\pi^+\pi^-$ pair combinations that both lie in the $\rho^0\rho^0$ signal mass window, we cannot distinguish which $\rho^0\rho^0$ mass combination is correct. In such cases, we select the $\pi^+\pi^-$ pair containing a high momentum $\pi^+(\pi^-)$ and a low momentum $\pi^-(\pi^+)$ as the correct combination; with this selection, 0.2% of the signal is incorrectly reconstructed according to the MC. For fitting, we randomly assign the $\pi^+\pi^-$ pairs to either $M_1(\pi^+\pi^-)$ or $M_2(\pi^+\pi^-)$ to symmetrize the 2-D invariant mass distribution. Therefore, the probability density functions

(PDF) for $M_1(\pi^+\pi^-)$ - $M_2(\pi^+\pi^-)$ are symmetric in both the $M_1(\pi^+\pi^-)$ and $M_2(\pi^+\pi^-)$ projections.

BACKGROUND SUPPRESSION

The dominant background is the continuum. To distinguish signal from the jet-like continuum background, we use modified Fox-Wolfram moments [19], which are combined into a Fisher discriminant. This discriminant is combined with PDFs for the cosine of the B flight direction in the CM and the distance in the z -direction between two B mesons to form a likelihood ratio $\mathcal{R} = \mathcal{L}_s / (\mathcal{L}_s + \mathcal{L}_{q\bar{q}})$. Here, \mathcal{L}_s ($\mathcal{L}_{q\bar{q}}$) is a likelihood function for signal (continuum) events that is obtained from the signal MC simulation (events in the sideband region $M_{bc} < 5.26$ GeV/ c^2). We also use the flavor tagging quality variable r provided by a tagging algorithm [20] that identifies the flavor of the accompanying B^0 meson in the $\Upsilon(4S) \rightarrow B^0\bar{B}^0$. The variable r ranges from $r = 0$ (no flavor discrimination) to $r = 1$ (unambiguous flavor assignment), and is used to divide the data sample into six r bins. Since the discrimination between signal and continuum events depends on the r -bin, we impose different requirements on \mathcal{R} for each r -bin. We determine the \mathcal{R} requirement so that it maximizes the figure-of-merit $N_s / \sqrt{N_s + N_{q\bar{q}}}$, where N_s ($N_{q\bar{q}}$) is the expected number of signal (continuum) events in the signal region ($|\Delta E| < 0.05$ GeV and 5.27 GeV/ $c^2 < M_{bc} < 5.29$ GeV/ c^2).

After applying all selection criteria, 17% of selected events have multiple $B^0 \rightarrow \rho^0\rho^0$ candidates. For these events we select a single candidate that having the smallest χ^2 value of the B^0 decay vertex reconstruction. The detection efficiency for the signal MC is calculated to be 7.11% (9.57%) for longitudinal (transverse) polarization.

ANALYSIS PROCEDURE

Since there are large overlaps between $B^0 \rightarrow \rho^0\rho^0$ and other signal decay modes in the $M_1(\pi\pi)$ - $M_2(\pi\pi)$ distribution, it is better to distinguish these modes using a simultaneous fit to a large $M_1(\pi\pi)$ - $M_2(\pi\pi)$ region. However, the correlations between $(\Delta E, M_{bc})$ and (M_1, M_2) for backgrounds and signals will lead to large uncertainties as the region in $M_1(\pi\pi)$ - $M_2(\pi\pi)$ used in a simultaneous fit increases. The $M_1(\pi\pi)$ - $M_2(\pi\pi)$ distribution is shown in Fig. 1 for Monte Carlo samples of non-resonant $B^0 \rightarrow 4\pi$, $B^0 \rightarrow \rho^0\pi\pi$, $B^0 \rightarrow \rho^0\rho^0$ decays, and the data. The analysis proceeds in three steps: we first measure the non-resonant $B^0 \rightarrow 4\pi$ branching fraction in area A, then measure the $B^0 \rightarrow \rho^0\pi\pi$ in area B by fixing the branching fraction of non-resonant $B^0 \rightarrow 4\pi$ determined in area A. Finally, we determine $B^0 \rightarrow \rho^0\rho^0$ and the other possible decay modes in area C by fixing the branching fractions of the non-resonant $B^0 \rightarrow 4\pi$ and $B^0 \rightarrow \rho^0\pi\pi$ decays. This procedure minimizes bias caused by unknown correlations between variables $(\Delta E, M_{bc})$ and variables (M_1, M_2) .

For the non-resonant $B^0 \rightarrow 4\pi$ branching fraction measurement, we use the nominal $\pi^+\pi^-$ mass region 1.05 GeV/ $c^2 < M_{1(2)}(\pi\pi) < 1.70$ GeV/ c^2 and 1.35 GeV/ $c^2 < M_{2(1)}(\pi\pi) < 1.70$ GeV/ c^2 (area A), in which only $B^0 \rightarrow a_1^\pm\pi^\mp$ and non-resonant $B^0 \rightarrow 4\pi$ signals having the same final state need to be considered. For the $B^0 \rightarrow \rho^0\pi\pi$ branching fraction measurement, we use events in the mass regions 1.30 GeV/ $c^2 < M_{1(2)}(\pi\pi) < 1.70$ GeV/ c^2 and 0.55 GeV/ $c^2 < M_{2(1)}(\pi\pi) < 0.95$ GeV/ c^2 (area B), in

which $B^0 \rightarrow a_1^\pm \pi^\mp$, non-resonant $B^0 \rightarrow 4\pi$ and $B^0 \rightarrow \rho^0 \pi \pi$ decays are included. The yields for $B^0 \rightarrow \rho^0 \rho^0$, $\rho^0 f_0$, $f_0 f_0$ and $f_0 \pi \pi$ decays are measured using a simultaneous fit in which the branching fractions of non-resonant $B^0 \rightarrow 4\pi$ and $B^0 \rightarrow \rho^0 \pi \pi$ in the mass region $0.55 \text{ GeV}/c^2 < M_{1,2}(\pi\pi) < 1.35 \text{ GeV}/c^2$ (area C) are fixed.

In all fits, we fix the branching fraction of $B^0 \rightarrow a_1^\pm \pi^\mp$ to the published value $(33.2 \pm 3.0 \pm 3.8) \times 10^{-6}$ [21]. Recently, Belle presented a preliminary result for the $B^0 \rightarrow a_1^\pm \pi^\mp$ branching fraction [22], which is consistent with BaBar's value. We also float the $B^0 \rightarrow a_1^\pm \pi^\mp$ yield in the fit; the result with its error is consistent with the assumed value.

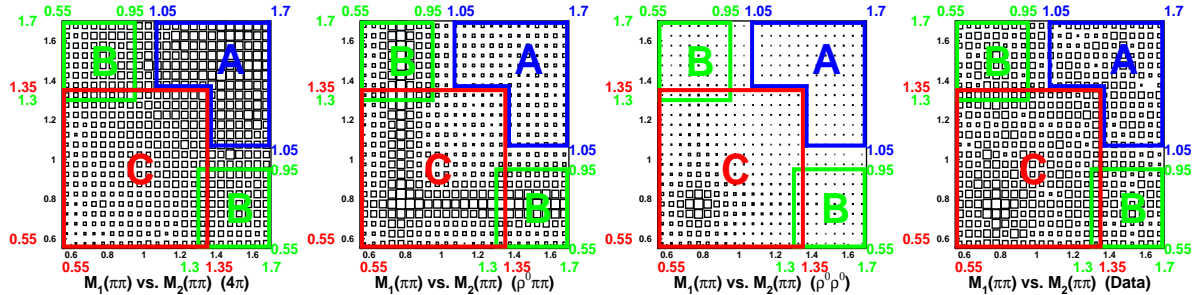


FIG. 1: $M_1(\pi\pi)$ - $M_2(\pi\pi)$ distributions in MC simulation of non-resonant $B^0 \rightarrow 4\pi$, $B^0 \rightarrow \rho^0 \pi \pi$, and $B^0 \rightarrow \rho^0 \rho^0$ decays, and the data, from left to right. Non-resonant $B^0 \rightarrow 4\pi$ and $B^0 \rightarrow \rho^0 \pi \pi$ MC decays are generated with 4- and 3-body phase space models.

The signal yields are extracted by performing extended unbinned maximum likelihood (ML) fits. In the fits, we use four dimensional (M_{bc} , ΔE , M_1 , M_2) information to measure the branching fraction of B^0 decays into non-resonant 4π , $\rho^0 \rho^0$, $\rho^0 f_0$, $f_0 f_0$ and $f_0 \pi \pi$, and two dimensional (M_{bc} , ΔE) information for the decay $B^0 \rightarrow \rho^0 \pi \pi$. We perform a 2D fit to extract the $\rho^0 \pi \pi$ yield since the $M_1(\pi\pi)$ - $M_2(\pi\pi)$ region used in the fit is expected to consist of $a_1^\pm \pi^\mp$, non-resonant 4π and $\rho^0 \pi \pi$ decays and no contributions from other resonant decay modes. We define the likelihood function

$$\mathcal{L} = \exp\left(-\sum_j n_j\right) \prod_{i=1}^{N_{\text{cand}}} \left(\sum_j n_j P_j^i\right), \quad (1)$$

where i is the event identifier, j indicates one of the event type categories for signals and backgrounds; n_j denotes the yield of the j -th category, and P_j^i is the probability density function (PDF) for the j -th category. For the 4D fits, the PDFs are a product of two smoothed two-dimensional functions: $P_j^i = P_j(M_{bc}^i, \Delta E^i, M_1^i, M_2^i) = f_{\text{smoothed}}(M_{bc}^i, \Delta E^i) \times f_{\text{smoothed}}(M_1^i, M_2^i)$. For the $B^0 \rightarrow \rho^0 \pi \pi$ branching fraction measurement, the PDFs are two-dimensional functions, i.e. $P_j^i = P_j(M_{bc}^i, \Delta E^i) = f_{\text{smoothed}}(M_{bc}^i, \Delta E^i)$.

For the signal modes, the smoothed functions $f_{\text{smoothed}}(M_{bc}^i, \Delta E^i)$ and $f_{\text{smoothed}}(M_1^i, M_2^i)$ are obtained from MC simulations. For the M_{bc} and ΔE PDFs, possible differences between the real data and the MC modeling are calibrated using a large control sample of $B^0 \rightarrow D^-(K\pi\pi)\pi^+$ decays. We find 16.2% (3.8%) of the reconstructed signal MC events are self-cross-feed (SCF) events for longitudinal (transverse) polarization; for SCF events at least one track from the decay $B^0 \rightarrow \rho^0 \rho^0$ is replaced by one from the accompanying B meson decay. We use different PDFs for the SCF events

and correctly reconstructed events, and employ the SCF fraction for a longitudinally polarized decay in the nominal fit. The uncertainty in the fraction of transversely polarized $B^0 \rightarrow \rho^0 \rho^0$ is taken into account as a systematic error.

For the continuum and charm B decay backgrounds, we use a linear function for ΔE , an ARGUS function [23] for M_{bc} and a two-dimensional smoothed function for M_1 - M_2 . The parameters of the linear function and ARGUS function for the continuum events are floated in the fit. Other parameters and shape of the M_1 - M_2 functions are obtained from MC simulations and fixed in the fit.

For the charmless B decay backgrounds, we construct four separate PDFs for $B^0 \rightarrow a_1^\pm \pi^\mp$, $B^+ \rightarrow \rho^+ \rho^0$, $B \rightarrow \rho^+ \rho^- + \rho \pi$ and other charmless B decays; all the PDFs are obtained using MC simulations. In the fit, while the yields of the $B^0 \rightarrow a_1^\pm \pi^\mp$, $B^+ \rightarrow \rho^+ \rho^0$ and $B \rightarrow \rho^+ \rho^- + \rho \pi$ are fixed to expected values obtained from measured branching fractions, the yield of other charmless B decays is floated.

MEASUREMENTS OF BRANCHING FRACTIONS

With the fitted signal yields $n_{\text{sig.}}$, we calculate the branching fraction \mathcal{B} using

$$\mathcal{B} = \frac{n_{\text{sig.}}}{N_{B\bar{B}} \cdot \epsilon_{\text{MC}} \cdot \epsilon_{\text{PID}}}, \quad (2)$$

where ϵ_{MC} is the overall reconstruction efficiency obtained using MC samples, ϵ_{PID} is a PID efficiency correction that takes into account the efficiency difference between data and MC, and $N_{B\bar{B}}$ is the number of $B\bar{B}$ pairs. The production rates of $B^+ B^-$ and $B^0 \bar{B}^0$ pairs are assumed to be equal. The PID efficiency correction is determined using an inclusive $D^{*+} \rightarrow D^0 \pi^+$, $D^0 \rightarrow K^- \pi^+$ data sample where the track momenta and polar angles are required to be consistent with those of $B^0 \rightarrow \rho^0 \rho^0$.

The statistical significance is defined as $\mathcal{S}_0 = \sqrt{-2 \ln(\mathcal{L}_0/\mathcal{L}_{\text{max}})}$, where \mathcal{L}_0 and \mathcal{L}_{max} are the likelihoods of the fits with the signal yield fixed at zero and at the fitted value, respectively.

The 90% confidence level (C.L.) upper limit is calculated from the equation

$$\frac{\int_0^N \mathcal{L}(x) dx}{\int_0^\infty \mathcal{L}(x) dx} = 90\%, \quad (3)$$

where x indicates likelihood variables corresponding to the yield, and N is the upper bound for the yield that includes 90% of the integral of the likelihood function.

The upper limit (UL) including systematic uncertainties is calculated by smearing the statistical likelihood function with a Gaussian, where the Gaussian width is the combination of two total systematic errors: one is independent of the branching fraction and the other is proportional to it. The significance including systematic uncertainties is calculated in the same way, but we only included the systematic errors related to signal yields in the convoluted Gaussian width.

The fitted yields and branching fractions with systematic errors are listed in Table I. Fig. 2 shows the projections of the data onto ΔE , M_{bc} , $M_1(\pi\pi)$ and $M_2(\pi\pi)$ for non-resonant $B^0 \rightarrow 4\pi$ decay in area A. Fig. 3 shows the projections of the data onto ΔE and M_{bc} for the $B^0 \rightarrow \rho^0 \pi\pi$ decay in area B. Fig. 4 shows the projections of the plots

for the $B^0 \rightarrow \rho^0 \rho^0$ decay in area C. We measure $B^0 \rightarrow \rho^0 \rho^0$ and non-resonant $B^0 \rightarrow 4\pi$ decays with 1.7σ and 2.2σ significance, respectively. There are no significant yields for $B^0 \rightarrow \rho^0 f_0$, $B^0 \rightarrow f_0 f_0$, $B^0 \rightarrow f_0 \pi\pi$ or $B^0 \rightarrow \rho^0 \pi\pi$ decays.

TABLE I: Fit results for each decay mode listed in the first column. The signal yields, reconstruction efficiency, significance including systematic uncertainties (\mathcal{S}), branching fractions (\mathcal{B}) and UL including systematic uncertainties are listed. For the yields and branching fractions, the first (second) error is statistical (systematic).

Mode	Yield	Eff.(%)	\mathcal{S}	$\mathcal{B}(\times 10^{-6})$	UL($\times 10^{-6}$) (90% C.L.)
Area A measurement:					
4π	$32.2 \pm 14.9^{+7.1}_{-4.7}$	0.61	2.1	$10.2 \pm 4.7^{+2.3}_{-1.5}$	<17.3
Area B measurement:					
$\rho^0 \pi\pi$	$-11.5 \pm 17.8^{+24.0}_{-15.0}$	0.86	0.0	–	<6.3
Area C measurement:					
$\rho^0 \rho^0$	$33.7 \pm 16.0^{+12.5}_{-13.2}$	7.11	1.8	$0.9 \pm 0.4^{+0.3}_{-0.4}$	<1.6
$\rho^0 f_0$	$3.6 \pm 11.7^{+7.3}_{-7.7}$	4.01	0.3	$0.2 \pm 0.6 \pm 0.4$	<1.0
$f_0 f_0$	$1.6 \pm 3.7 \pm 2.9$	2.23	0.4	$0.1 \pm 0.3 \pm 0.3$	<0.8
$f_0 \pi\pi$	$-6.0 \pm 19.7^{+23.0}_{-16.6}$	0.71	0.0	–	<8.6

ρ^0 HELICITY

We perform an angular analysis of $B^0 \rightarrow \rho^0 \rho^0$ using the sum of two ρ^0 helicity angle distributions for the signal candidates having $M_1(\pi\pi)$ and $M_2(\pi\pi)$ values in the signal region ($0.626 \text{ GeV}/c^2 < M_{1,2}(\pi\pi) < 0.926 \text{ GeV}/c^2$). The ρ^0 helicity angle is defined as the angle between the π^+ direction and the B^0 direction in the ρ^0 rest frame. Fig. 5 shows the sum of the two ρ^0 helicity angle distributions; each bin has a B^0 yield obtained from a ΔE - M_{bc} fit that does not distinguish whether the B^0 decays into $\rho^0 \rho^0$, $a_1^\pm \pi^\mp$ or 4π . We fix the fractions of the three B^0 decays modes to values obtained from the the 4-D ML fit in area C. In the helicity angle fit, we vary the longitudinal polarization fraction for the $B^0 \rightarrow \rho^0 \rho^0$ component. A χ^2 fit yields a longitudinal polarization fraction for $B^0 \rightarrow \rho^0 \rho^0$ of $f_L = 0.6 \pm 0.2$. The statistical error is obtained from a MC pseudo-experiment study, since the two ρ^0 helicity angle distributions are correlated.

SYSTEMATIC ERROR

The main systematic uncertainty for the branching fraction of non-resonant $B^0 \rightarrow 4\pi$ decay is the uncertainty of the $B^0 \rightarrow a_1^\pm \pi^\mp$ branching fraction. The main systematic uncertainties for the $B^0 \rightarrow \rho^0 \pi\pi$ branching fraction are the uncertainties of the non-resonant $B^0 \rightarrow 4\pi$ and $B^0 \rightarrow a_1^\pm \pi^\mp$ branching fractions. For $B^0 \rightarrow \rho^0 \rho^0$ decay, the main sources of systematic uncertainties include the uncertainties on the branching fractions of $B^0 \rightarrow a_1^\pm \pi^\mp$, non-resonant $B^0 \rightarrow 4\pi$, $B^0 \rightarrow \rho^0 \pi\pi$, $B^\pm \rightarrow \rho^0 \rho^\pm$ and $B^0 \rightarrow \rho^0 K^{*0}$.

We vary the branching fractions of $B^0 \rightarrow a_1^\pm \pi^\mp$ (33.2 ± 4.8 , in units of 10^{-6}) [21] and $B^\pm \rightarrow \rho^0 \rho^\pm$ (18.2 ± 3.0) [24] by their $\pm 1\sigma$ errors. On the other hand, we vary the

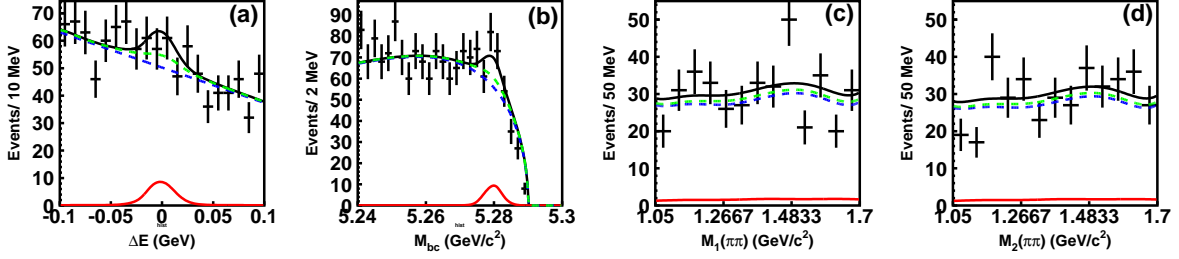


FIG. 2: Area A: projections of the four dimensional fit onto (a) ΔE , (b) M_{bc} , (c) $M_1(\pi\pi) \in (1.05, 1.7)$ GeV/c^2 and (d) $M_2(\pi\pi) \in (1.05, 1.7)$ GeV/c^2 . For the ΔE projection: $5.27 \text{ GeV}/c^2 < M_{bc} < 5.29 \text{ GeV}/c^2$; for the M_{bc} projection: $|\Delta E| < 0.05 \text{ GeV}$; for the $M_{1(2)}(\pi\pi)$ projection: $|\Delta E| < 0.05 \text{ GeV}$ and $5.27 \text{ GeV}/c^2 < M_{bc} < 5.29 \text{ GeV}/c^2$ and $1.35 \text{ GeV}/c^2 < M_{2(1)}(\pi\pi) < 1.70 \text{ GeV}/c^2$. The fit result is shown as the thick solid curve; the red solid curve represents the signal component, non-resonant $B^0 \rightarrow 4\pi$ decay; the blue dashed and and green dashed curves represent the cumulative background components from continuum plus $b \rightarrow c$ backgrounds, and charmless B decays.

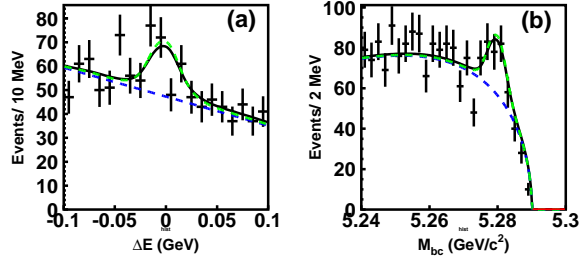


FIG. 3: Area B: projections of the two dimensional fit onto (a) ΔE , (b) M_{bc} . For the ΔE projection: $5.27 \text{ GeV}/c^2 < M_{bc} < 5.29 \text{ GeV}/c^2$; for the M_{bc} projection: $|\Delta E| < 0.05 \text{ GeV}$. The fit result is shown as the thick solid curve; the $B^0 \rightarrow \rho^0\pi\pi$ component cannot be seen here because of its negative yield; the blue dashed and and green dashed curves represent the cumulative background components from continuum plus $b \rightarrow c$ backgrounds, and charmless B decays.

branching fractions of $B^0 \rightarrow \rho^0 K^{*0}$, non-resonant $B^0 \rightarrow 4\pi$ and $B^0 \rightarrow \rho^0\pi\pi$ in the range $(0, 7.2) \times 10^{-6}$ [24], $(0, 15.4) \times 10^{-6}$ (area A measurement) and $(0, 4.1) \times 10^{-6}$ (area B measurement), respectively, because these branching fractions are not measured with high significance. The fits are repeated and the differences between the results and the nominal fit values are taken as systematic errors.

According to MC, the signal SCF fractions are 16.2% for $B^0 \rightarrow \rho^0\rho^0$, 10.6% for $B^0 \rightarrow \rho^0 f_0$, 7.3% for $B^0 \rightarrow f_0 f_0$, 12.4% for $B^0 \rightarrow f_0\pi\pi$, 10.8% for $B^0 \rightarrow \rho^0\pi\pi$ and 11.1% for non-resonant $B^0 \rightarrow 4\pi$. We estimate a systematic uncertainty for the signal SCF by setting its fraction to zero. A systematic error for the longitudinal polarization fraction of $B^0 \rightarrow \rho^0\rho^0$ is obtained by changing the fraction from the nominal value $f_L = 1$ to our measured value $f_L = 0.6$. A MC study indicates that the fit biases are +7 events for $B^0 \rightarrow \rho^0\rho^0$, +1 event for $B^0 \rightarrow \rho^0 f_0$, -1 event for $B^0 \rightarrow f_0 f_0$, -3 events for $B^0 \rightarrow f_0\pi\pi$

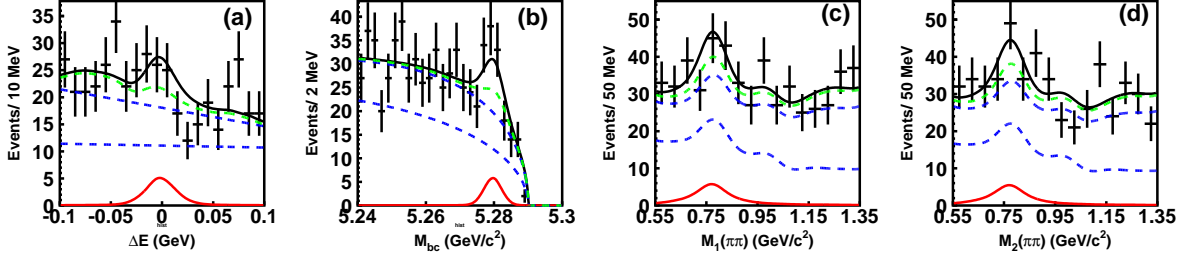


FIG. 4: Area C: projections of the four dimensional fit onto (a) ΔE , (b) M_{bc} , (c) $M_1(\pi\pi) \in (0.55, 1.35) \text{ GeV}/c^2$ and (d) $M_2(\pi\pi) \in (0.55, 1.35) \text{ GeV}/c^2$. For the ΔE projection: $5.27 \text{ GeV}/c^2 < M_{bc} < 5.29 \text{ GeV}/c^2$; for the M_{bc} projection: $|\Delta E| < 0.05 \text{ GeV}$; for the $M_{1(2)}(\pi\pi)$ projection: $|\Delta E| < 0.05 \text{ GeV}$ and $5.27 \text{ GeV}/c^2 < M_{bc} < 5.29 \text{ GeV}/c^2$ and $0.626 \text{ GeV}/c^2 < M_{2(1)}(\pi\pi) < 0.926 \text{ GeV}/c^2$. The fit result is shown as the thick solid curve; the red solid line represents the signal component, $B^0 \rightarrow \rho^0 \rho^0$ decay; the blue dashed, dash-dotted and green dashed curves represent, respectively, the cumulative background components from continuum processes, $b \rightarrow c$ decays, and charmless B backgrounds.

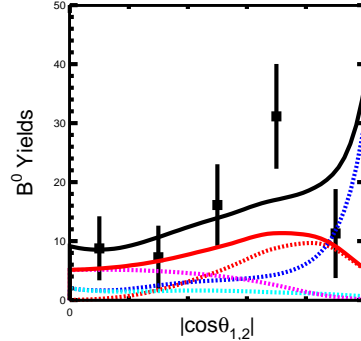


FIG. 5: Sum of two ρ^0 helicity angle distributions for background-subtracted events in the region $(0.626 \text{ GeV}/c^2 < M_{1,2}(\pi\pi) < 0.926 \text{ GeV}/c^2)$. The points with error bars represent the B^0 yields obtained from ΔE - M_{bc} ML fits for each helicity angle interval. The black overlaid curve is the sum of expected distributions from MC. The blue, cyan, red and magenta dashed curves represent the $B^0 \rightarrow a_1\pi$, non-resonant $B^0 \rightarrow 4\pi$, longitudinally and transversely polarized $B^0 \rightarrow \rho^0 \rho^0$ decays, respectively. The red solid curve represents the sum of two polarized $B^0 \rightarrow \rho^0 \rho^0$ decays.

and +6 events for non-resonant $B^0 \rightarrow 4\pi$. We find that fit biases occur due to the correlations between the two sets of variables ($\Delta E, M_{bc}$) and (M_1 and M_2), which are not taken into account in our fit. We correct the yields in the fit for these biases and include the corrections as systematic errors.

Systematic uncertainties for the ΔE - M_{bc} PDFs used in the fit are estimated by performing the fits while varying the signal peak positions and resolutions by $\pm 1\sigma$. Systematic uncertainties for the M_1 - M_2 PDFs are estimated in a similar way. We vary the mean and width of the ρ^0 and f_0 masses in the M_1 - M_2 PDFs for the decay modes $B^0 \rightarrow \rho^0 \rho^0$, $B^0 \rightarrow \rho^0 f_0$, $B^0 \rightarrow f_0 f_0$, and $B^0 \rightarrow f_0 \pi\pi$. For the non-resonant $B^0 \rightarrow 4\pi$, other rare B

decay, $b \rightarrow c$ and continuum backgrounds, we vary their M_1 - M_2 PDF shapes, repeat the fits, and take the deviations from the central values as the systematic errors.

We test the possible interference between $B^0 \rightarrow a_1^\pm \pi^\mp$, non-resonant $B^0 \rightarrow 4\pi$ and $B^0 \rightarrow \rho^0 \rho^0$ by toy MC. We add a simple interference model to the toy MC generation, which is, for $\rho^0 \rightarrow \pi^+ \pi^-$ decay, modified from a relativistic Breit-Wigner function to

$$\left| \frac{1}{m^2 - m_0^2 + im_0\Gamma} + Ae^{-i\delta} \right|^2 = A^2 + 2A \left[\frac{(m^2 - m_0^2) \cos \delta - \Gamma m_0 \sin \delta}{(m^2 - m_0^2)^2 + (\Gamma m_0)^2} \right] + \frac{1}{(m^2 - m_0^2)^2 + (\Gamma m_0)^2}, \quad (4)$$

where A and δ are the interference amplitude and phase, m_0 and Γ are the ρ^0 mass and width, respectively. We assume that the interference term due to the amplitudes for $B^0 \rightarrow a_1^\pm \pi^\mp$ and non-resonant $B^0 \rightarrow 4\pi$ decays is constant in the $B^0 \rightarrow \rho^0 \rho^0$ signal region. Since the magnitude of the interfering amplitude and relative phase are not known, we uniformly vary these parameters and perform a fit in each case to measure the deviations from the incoherent case. The mean deviation is calculated, and we add and subtract the r.m.s. of the distribution of deviations from this value to obtain the systematic uncertainty. The interference systematic for $B^0 \rightarrow \rho^0 \rho^0$ decay is $({}^{+12.6}_{-4.8})\%$.

The systematic errors for the efficiency arise from the tracking efficiency, particle identification (PID) and \mathcal{R} requirement. The systematic error due to the track finding efficiency is estimated to be 1.3% per track using partially reconstructed D^* events. The systematic error due to the pion identification (PID) is 1.2% per track estimated using an inclusive D^* control sample. The \mathcal{R} requirement systematic error is determined from the efficiency difference between data and MC using a $B^0 \rightarrow D^+(K\pi\pi)\pi^-$ control sample. Table II summarizes the sources of systematic uncertainties and their quadratic sum for each of the items. The overall relative systematic errors are $({}^{+37.1}_{-39.1})\%$ for the $B^0 \rightarrow \rho^0 \rho^0$ decay and $({}^{+22.2}_{-14.5})\%$ for non-resonant $B^0 \rightarrow 4\pi$ decay.

SUMMARY

In summary, we measure the branching fraction of $B^0 \rightarrow \rho^0 \rho^0$ to be $(0.9 \pm 0.4{}^{+0.3}_{-0.4}) \times 10^{-6}$ with 1.8σ significance; the 90% confidence level upper limit including systematic uncertainties is $\mathcal{B}(B^0 \rightarrow \rho^0 \rho^0) < 1.6 \times 10^{-6}$. Since no significant signal is found, we have assumed this mode is a longitudinally polarized decay ($f_L = 1$), to obtain the most conservative upper limit. For $f_L = 0.0$, we obtain the central value of $\mathcal{B}(B^0 \rightarrow \rho^0 \rho^0) = 0.6 \times 10^{-6}$. Measurements of polarization and asymmetry in $B^0 \rightarrow \rho^0 \rho^0$ will be needed to improve the precision of the ϕ_2 constraint.

On other hand, we find an excess in non-resonant $B^0 \rightarrow 4\pi$ decay with 2.1σ significance. We measure the branching fraction and a 90% confidence level upper limit for non-resonant $B^0 \rightarrow 4\pi$ decay to be $(10.2 \pm 4.7{}^{+2.3}_{-1.5}) \times 10^{-6}$ and $\mathcal{B}(B^0 \rightarrow 4\pi) < 17.3 \times 10^{-6}$. This contribution was not taken into account in previous measurements of $B^0 \rightarrow \rho^0 \rho^0$ [9]. We find no significant signal for the decays $B^0 \rightarrow \rho^0 f_0$, $B^0 \rightarrow f_0 f_0$, $B^0 \rightarrow f_0 \pi\pi$ and $B^0 \rightarrow \rho^0 \pi\pi$; the corresponding upper limits are listed in Table I.

ACKNOWLEDGMENTS

We thank the KEKB group for the excellent operation of the accelerator, the KEK cryogenics group for the efficient operation of the solenoid, and the KEK computer group

TABLE II: Summary of systematic errors (%) for the branching fraction measurements. f_L and f_{SCF} are the fractional uncertainties for longitudinal polarization and self-cross-feed.

Source	4π	$\rho^0\pi\pi$	$\rho^0\rho^0$	ρ^0f_0	f_0f_0	$f_0\pi\pi$
Fitting PDF	± 6.8	± 9.6	± 13.1	± 197.7	± 159.4	± 194.4
$\mathcal{B}(B^0 \rightarrow a_1\pi)$	± 3.7	$+100.0$ -96.5	$+4.7$ -5.3	$+2.8$ -5.6	$+18.8$ -12.5	$+48.3$ -51.7
$\mathcal{B}(B^0 \rightarrow 4\pi)$	—	$+181.7$ -86.1	$+14.5$ -7.1	$+16.7$ -52.8	$+37.5$ -50.0	$+326.7$ -146.7
$\mathcal{B}(B^0 \rightarrow \rho^0\pi\pi)$	—	—	-28.5	-55.6	$+31.3$	-108.3
$\mathcal{B}(B^\pm \rightarrow \rho^0\rho^\pm)$	—	0.0	± 0.6	± 2.8	0.0	0.0
$\mathcal{B}(B^0 \rightarrow \rho^0 K^{*0})$	—	—	$+1.5$	$+13.9$	0.0	-16.7
f_L	—	—	-11.1	—	—	—
f_{SCF}	-9.6	$+13.9$	-15.7	-11.1	$+18.8$	$+3.3$
Interference	—	—	$+12.6$ -4.8	—	—	—
Fit bias correction	$+19.6$ -3.1	± 8.7	$+22.0$ -3.0	$+36.0$ -27.8	± 62.5	$+16.7$ -48.3
Tracking	± 4.2	± 4.3	± 5.1	± 5.0	± 4.4	± 4.3
PID	± 4.1	± 4.2	± 4.9	± 4.6	± 4.5	± 4.2
\mathcal{R} requirement	± 3.4	± 3.4	± 3.4	± 3.4	± 3.4	± 3.4
$N_{B\bar{B}}$	± 1.3	± 1.3	± 1.3	± 1.3	± 1.3	± 1.3
Sum(%)	$+22.2$ -14.5	$+208.4$ -130.2	$+37.1$ -39.1	$+202.3$ -214.4	$+180.2$ -179.0	$+383.7$ -276.4

and the National Institute of Informatics for valuable computing and Super-SINET network support. We acknowledge support from the Ministry of Education, Culture, Sports, Science, and Technology of Japan and the Japan Society for the Promotion of Science; the Australian Research Council and the Australian Department of Education, Science and Training; the National Science Foundation of China and the Knowledge Innovation Program of the Chinese Academy of Sciences under contract No. 10575109 and IHEP-U-503; the Department of Science and Technology of India; the BK21 program of the Ministry of Education of Korea, the CHEP SRC program and Basic Research program (grant No. R01-2005-000-10089-0) of the Korea Science and Engineering Foundation, and the Pure Basic Research Group program of the Korea Research Foundation; the Polish State Committee for Scientific Research; the Ministry of Education and Science of the Russian Federation and the Russian Federal Agency for Atomic Energy; the Slovenian Research Agency; the Swiss National Science Foundation; the National Science Council and the Ministry of Education of Taiwan; and the U.S. Department of Energy.

-
- [1] N. Cabibbo, Phys. Rev. Lett. **10**, 531 (1963); M. Kobayashi, T. Maskawa, Prog. Theor. Phys. **49**, 652 (1973).
[2] M. Gronau and D. London, Phys. Rev. Lett. **65**, 3381 (1990).
[3] H. Ishino *et al.* (Belle Collaboration), Phys. Rev. Lett. **98** 211801 (2007); B. Aubert *et al.* (BaBar Collaboration), Phys. Rev. Lett. **99** 021603 (2007).
[4] A. Kusaka *et al.* (Belle Collaboration), Phys. Rev. Lett. **98** 221602 (2007); B. Aubert *et al.*

- (BaBar Collaboration), arXiv:hep-ex/0703008 Phys. Rev. D. (to be published).
- [5] A. Somov *et al.* (Belle Collaboration), Phys. Rev. D **76**, 011104 (2007); B. Aubert *et al.* (BaBar Collaboration), arXiv:0705.2157 [hep-ex], submitted to Phys. Rev. D.
 - [6] H. Li, S. Mishima Phys. Rev. D **73** 114014 (2006).
 - [7] M. Beneke, J. Rohrer, D. Yang, arXiv:hep-ph/0612290.
 - [8] W. Zou, Z. Xiao, Phys. Rev. D **72** (2005) 094026, arXiv:hep-ph/0507122.
 - [9] B. Aubert, *et al.* (BaBar Collaboration), Phys. Rev. Lett. **98**, 111801 (2007).
 - [10] K. Berkelman, *Hadronic Decays*, in *B Decays* ed. by S. Stone, World Scientific, Singapore (1992).
 - [11] W. Adam *et al.* (DELPHI Collaboration), Z. Phys. C72: 207-220 (1996); P. Abreu *et al.* (DELPHI Collaboration), Phys. Lett. B357: 255-266 (1995).
 - [12] S. Kurokawa and E. Kikutani, Nucl. Instrum. and Methods Phys. Res. Sect. A **499**, 1 (2003), and other papers included in this volume.
 - [13] A. Abashian, *et al.* (Belle Collaboration), Nucl. Instrum. and Methods Phys. Res. Sect. A **479**, 117 (2002).
 - [14] Z. Natkaniec *et al.* (Belle SVD2 Group), Nucl. Instrum. and Methods Phys. Res. Sect. A **560**, 1 (2006).
 - [15] D.J. Lange, Nucl. Instr. and Meth. A**462**, 152 (2001)
 - [16] E. Barberio and Z. Was, Comput. Phys. Commun. **79**, 291 (1994); P. Golonka and Z. Was, arXiv:hep-ph/0506026. We use PHOTOS version 2.13 allowing the emission of up to two photons, with an energy cut-off at 1% of the energy available for photon emission (i.e. approximately 26 MeV for the first emitted photon). PHOTOS also takes into account interference between charged final-state particles.
 - [17] T. Sjöstrand, Comput. Phys. Commun.**82**, 74 (1994); T. Sjöstrand and M. Bengtson, Comput. Phys. Commun.**43**, 367 (1987); T. Sjöstrand, Comput. Phys. Commun.**39**, 347 (1986).
 - [18] R. Brun *et al.*, GEANT 3.21, CERN Report DD/EE/841, 1984.
 - [19] G. C. Fox and S. Wolfram, Phys. Rev. Lett. **41** 1581 (1978). The modified moments used in this paper are described in S. H. Lee *et al.* (Belle Collaboration), Phys. Rev. Lett. **91**, 261801 (2003).
 - [20] H. Kakuno *et al.*, Nucl. Instr. and Meth. A **533**, 516 (2004).
 - [21] BaBar Collaboration, B. Aubert *et al.*, Phys. Rev.Lett. **97**, 051802 (2006).
 - [22] K. Abe *et al.* (Belle Collaboration), arXiv:0706.3279.
 - [23] H. Albrecht *et al.* (ARGUS Collaboration), Phys. Lett. B **241**, 278 (1990).
 - [24] E. Barberio *et al.* (Heavy Flavor Averaging Group), arXiv:0704.3575 [hep-ex] and online update for winter 2007 at <http://www.slac.stanford.edu/xorg/hfag/rare/index.html>